ARMA 16-792

Application of State of the Art Hydraulic Fracture Modelling Techniques for Safe-Optimized Design and for Enhanced Production

Profit, M.L., Dutko, M., Yu, J., Armstrong, J. and Parfitt, D.
Rockfield Global Technologies, Swansea, SA1 8AS, UK

Mutlu, U.
Rockfield Global Technologies America LLC, Houston, Texas, USA

ABSTRACT: This paper presents a number of emerging applications of hydraulic fracture initiation, propagation and interaction models. In the oil industry fracture design engineers often model hydraulic fracturing using 2D approximations but the physical process is inherently 3D and some very important aspects are lost during the model simplification, such as the means to impose a full 3D initial stress state and the capability of the fracture to propagate and potentially curve in an evolving complex stress state. A mode-1 3D hydraulic fracturing methodology is developed within an adaptive Finite Element Method (FEM) and Discrete Element Method (DEM) framework for generic fracture shapes. The fracture insertion process is based on a geometry update procedure rather than the more traditional DE approach of splitting elements along their edges or through the element itself. This leads to better control of the mesh quality and an improved performance of the numerical scheme. The applications include curving fracture paths and potentially connecting fractures from a multi-well stimulation stage.

1. INTRODUCTION

Hydraulic fracturing is a complex engineering process (Economides and Nolte, 2000) and understanding its key aspects are essential to a fracking design engineer whose main goal is to obtain a designed fracture complexity in the target reservoir (Cipolla et al, 2010; Economides and Nolte, 2000). A number of the complexities are inherent to hydraulic fracturing; such as material heterogeneity, local variations in stress and inadequacies in knowing the precise location of potentially several pre-existing fracture sets (King, 2010). Within a numerical framework (such as adaptive Finite Element (FE) (Zienkiewicz et al, 2005; Belytschko et al, 2000) and Discrete Element (DE) (Munjiza, 2004) methods) each of these knowledge gaps can be explored and their role in hydraulic fracturing better understood. In this paper enhanced production refers to the increase in fracture complexity.

The first attempts at quantifying hydraulic fracture almost exclusively centered on analytical schemes which provide a way of understanding some simple relationships between key variables such as fluid pressures and fracture widths (Yew and Weng, 2015). This simplicity comes at the cost of ignoring some of the major complexities which are observed in many hydraulic fracture jobs.

With the advent of more powerful computer architecture, sophisticated numerical schemes now offer tractable solutions to fully 3D models. The computational cost is still high but complemented with parallel processing practical simulation times are achievable and provide an essential guide in understanding the propagation of hydraulic fractures in complex evolving stress fields (Davies et al, 2012).

This prime focus of this paper is 3D hydraulic fracturing and the methodology follows a combined geomechanically coupled Finite and Discrete Element method, with interactions between the following fields (Lewis and Schrefler, 1998; Labao, 2007):

- Formation stresses;
- Pore fluid flow in the formation;
- Fracking fluid flow in the fracture region.

A key advancement in the present work is 3D fracture insertion based on geometry rather than mesh update procedures. Standard DEM techniques involve splitting a mesh either along element edges (see Fig. 1(b)) or through the element itself (see Fig. 1(c)) (Klerck, 2000). As an explicit solver is used to update the formation stresses the mesh quality is an essential part in determining the robustness of the numerical scheme (Wu and Giu, 2012).

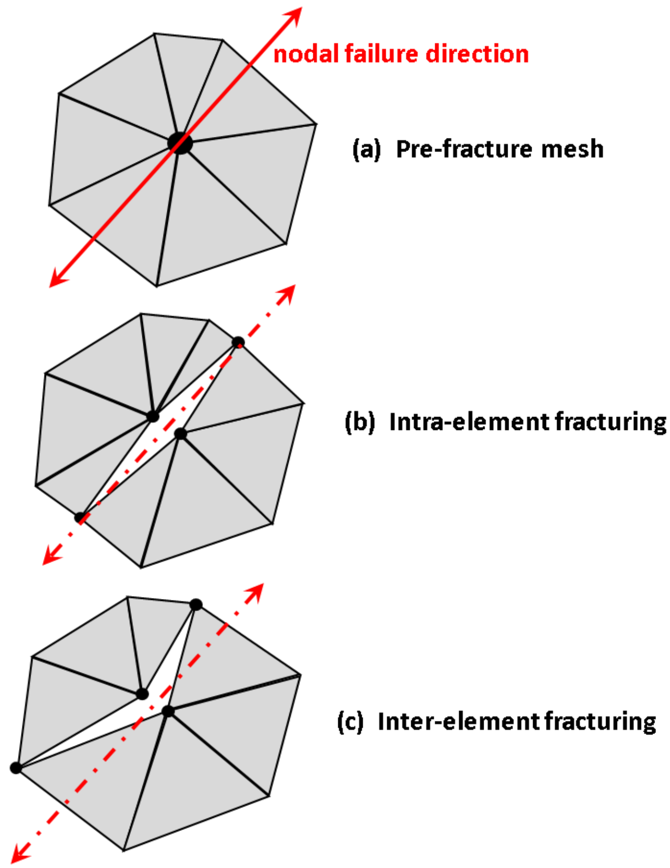

Fig. 1. Classical intra-element and inter-element fracturing

In principle for stiff reservoir rocks the material strain should remain relatively low and hence the mesh distortion should likewise undergo small changes. However, when mesh splitting techniques are used, particularly those where the cut is through the element itself, this behaviour is no longer guaranteed and the conditionally stable time step could drop to a prohibitively low value. By taking a geometry update approach (see Fig. 8 and Fig 9 for details), the mesh quality is maintained throughout a hydraulic fracture analysis with no significant drop in the time step value. Furthermore, a local remeshing scheme is performed at the fracture tip which saves on a potentially large number of computationally expensive 3D global remeshes.

The new 3D hydraulic fracture technology is implemented in the software package ELFEN (Rockfield Software Ltd, UK) and is called ELFEN TGR (Rockfield Software Ltd, 2014). This paper provides an overview of the methodology along with a number of examples illustrating the performance of the new technology: namely, curving fracture paths and potentially connecting fractures from a multi-well hydraulic stimulation stage.

2. KEY MODELLING ASPECTS

2.1. Overall Modelling Methodology

From standard hydraulic field practice, the core ELFEN TGR software is divided into 5 key stages (Rockfield Software Ltd, 2014):

- **(i)** Initialisation of model stresses, pore and fracking fluid pressures. This model could include complex Discrete Fracture Network (DFN) sets which requires initialisation of contact stresses prior to any hydraulic fracturing;
- **(ii)** Pad hydraulic fracturing;
- **(iii)** Slurry hydraulic fracturing;
- **(iv)** Flowblack and clean-up of the fractured region.
- **(v)** Gas production.

Three sets of governing equations are solved simultaneously (Gordeliey, 2013; Huang et al, 2001; Labao, 2007):

- **(i)** Stress balance between external loads (i.e. for this class of problem it is mainly the fracking fluid pressure acting along the fracture surfaces) and combined mechanical and pore fluid stresses of the rock formation (structure field);
- **(ii)** Porous flow in the rock formation (seepage field);
- **(iii)** Fluid flow in the fracture region (network field).

This paper focuses on the 3D implementation of stages 1 and 2 with the remaining stages beyond the scope of this paper. The hydraulic stimulation of tight gas reservoirs is the main target of this application. To fully capture the physical behaviour of this system would require a complex multi-phase fluid flow simulator due to the intricate interactions between the invading fracture fluid and the in-situ-reservoir gas. Owing to the high compressibility of gas inside the shale pore space, it is assumed that the fluid pressure change in the formation is negligible, so in effect the mechanical response of the formation evolves under the drained assumption.

2.2. Geomechanical Coupling Method

The main governing equations are derived assuming:

- **(i)** Equilibrium of stresses with an appropriate constitutive model which is able to capture both tensile and shear failure; the main fracturing mode is considered tensile.
- **(ii)** Mass conservation of fluid flow inside the fracture region with a flow constitutive response able to recover parallel plate flow theory. This leads to the well-known cubic flow rule. Other influences, such as the fracture surface roughness, is also included in the fluid flow models (Rockfield Software Ltd, 2014).

The governing equation for the solid field is given by (Labao, 2007):

$$div(\boldsymbol{\sigma}' - \alpha_r(\phi)\mathbf{m}p_s) + \rho_B\mathbf{g} = 0 \qquad (1)$$

where $\boldsymbol{\sigma}'$ is the effective stress tensor, α_r is the reservoir Biot coefficient which can be a function of its porosity ϕ, $\mathbf{m}$ is the identity tensor, p_s is the pore fluid pressure in the reservoir, ρ_B is the wet bulk density and $\mathbf{g}$ is the gravity vector. Similarly, the governing equation for the fracture fluid flow field is given by (Labao, 2007):

$$\frac{d}{dx}\left[\frac{\kappa_{fr}}{\mu_f}\left\{\frac{dp_n}{dx} + \rho_f\mathbf{g}\right\}\right] = S_{fr}\frac{dp_n}{dt} + \alpha_f(\Delta\dot{e_\varepsilon}) \qquad (2)$$

where κ_{fr} is the intrinsic permeability of the fractured region, μ_f is the viscosity of the fracturing fluid, p_n is the fracturing fluid pressure, ρ_f is the density of the fracturing fluid, S_{fr} is the storage coefficient which measures the effective compressibility of the fractured region when a fluid is present, α_f is the fractured region Biot coefficient and $\Delta\dot{e_\varepsilon}$ is the aperture strain rate. If parallel plate theory is assumed then the intrinsic permeability of the fractured region is given by:

$$\kappa_{fr} = e^2/12 \qquad (3)$$

where e is the fracture aperture. The storage term is given by:

$$S_{fr} = (1/e)\left[\left(1/K_n^{fr}\right) + \left(e/K_f^{fr}\right)\right] \qquad (4)$$

where K_n^{fr} is the fracture normal stiffness and K_f^{fr} is the bulk modulus of the fracturing fluid. A cartoon sketch of the modelling idealization is shown in Fig. 2.

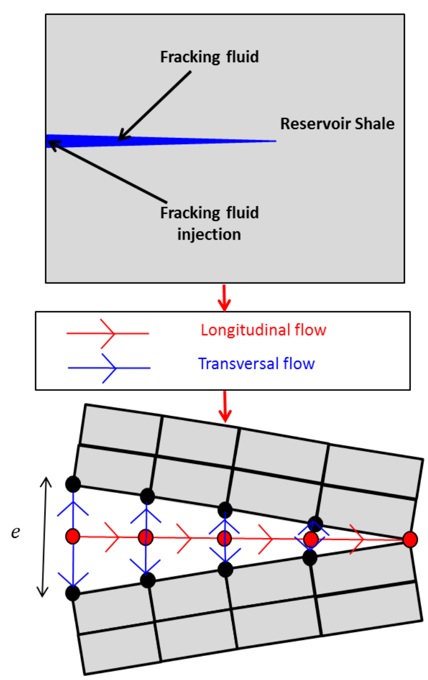

Fig. 2. Modelling idealisation

An essential point which has ramifications for the 3D fracture insertion procedure is the link between the network elements (i.e. the red bar elements in Fig. 2) and the fracture surface nodes. There must be a parent-child topological relationship or one-to-one mapping between these nodes to honour the overall computational methodology.

2.3. *Finite Element Discretisation*

The governing equations shown in Eq. (1). and Eq. (2). are discretised using the finite element method. More details on the final discretised matrix and vector expressions can be found in Profit et al, 2015.

2.4. *Coupling Scheme*

A staggered coupling scheme is implemented in which the mechanical governing equation (Eq. (1).) is solved explicitly and the fracture fluid flow governing equation (Eq. (2).) is solved implicitly. This implies that in an actual hydraulic fracture simulation there are many more explicit time steps per implicit time step and hence on the mechanical field the fracture fluid pressure needs to be updated between coupling stations (Profit et al, 2015**)**.

2.5. *Fracking Fluid Flow*

In hydraulic fracture jobs typically both Newtonian and non-Newtonian fluids are used, so the viscosity μ_f defined in Eq. (2). can be either constant or variable as a function of the shear strain rate. For non-linear fracturing fluids the rheological behaviour is represented via the power law model:

$$\tau = K\gamma^n \qquad (5)$$

where τ is the fracturing fluid shear stress, K is the power law consistency index, γ is the shear strain rate and n is the power law exponent. The non-linear fracturing fluid model is formulated from the generialised Navier-Stokes equation with the relevant parallel plate flow boundary conditions imposed. Shear-thinning gels are used in practice so the exponent term n is typically less than 1.

During hydraulic fracturing it is not untypical for there to be a significant amount of fluid loss even when the formation rock is a tight or low porosity shale. The precise reason for this behaviour is not known with some hypotheses including the invasion of fracturing fluid into fissures adjacent to the main fracture and capillary action due to the small pore throat radii of the shale grains. Whatever the exact cause one key effect of the fluid loss is a drop in fracture fluid pressure as the fracture propagates; so to ensure there is one-to-one mapping between the amount of fluid inside the fracture region and the fracture volume generated, it is essential that a leak-off facility is included in the software. The leak-off models implemented are the 1D fluid flow functions proposed by Carter (Rockfield Software Ltd, 2014; Williams, 1970).

2.6. *Material Model*

The material model takes a Continuum Damage Mechanics (CDM) approach with strain-softening behaviour in a preferred 1D crack band direction. The preferred direction is dependent on the principal stresses. It is assumed that orthogonal effects in the brittle materials are small during directional material modelling so there is no coupling between damage in one Cartesian direction and the remaining directions. The smeared crack model provides a solid framework for directional softening within a continuum methodology.

A 1D uniaxial continuum extensional stress-strain graph for a brittle is shown in Fig. 3 (ε_0 and ε_f are the uniaxial yield and failure strains respectively). The elastic response is governed in the standard way via the Young's modulus E and Poisson's ratio. Softening behaviour is defined via the tensile strength f_t and fracture energy G_f with an element characteristic length C_l included to account for objective energy dissipation in arbitrary meshes (Bazant and Planas, 1997; Crook et al, 2003). More details on the material model can be found in Klerck, 2000.

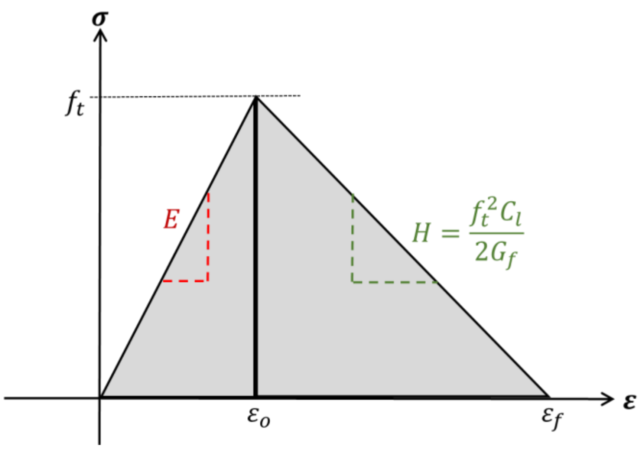

Fig. 3. 1D uniaxial continuum damage mechanics response.

2.7. *Fracture Geometry Insertion Procedure*

The insertion methodology builds on a previous 2D implementation which is described in Profit et al, 2015. The 3D hydraulic fracture insertion or propagation is divided into 6 stages:

1. *Prediction*: Determining the growth of existing hydraulic fractures;
2. *Stitching*: Converting the discrete model into a continuum model;
3. *Insertion*: Adding the new fracture geometry to the model;
4. *Meshing*: Internal local re-meshing of the affected area;
5. *Expansion*: Converting the continuum model back to a discrete model;
6. *Mapping*: Map all the analysis variables to the new model.

Each of these stages will be described in more detail in this Section. To clarify later discussions, a typical 3D ELFEN TGR model set-up is shown in Fig. 4 and Fig. 5. The initial mesh is shown in Fig. 4 with a profile view of the model, i.e. the outer boundaries of geometry entities, shown in Fig. 5.

The key point here is the inclusion of an initial planar starter crack in the model from which the hydraulic fracture will originally propagate. Fluid is pumped into this crack at a specified flow rate which typically results in tensile damage forming around its boundary. This can eventually lead to fracture insertion.

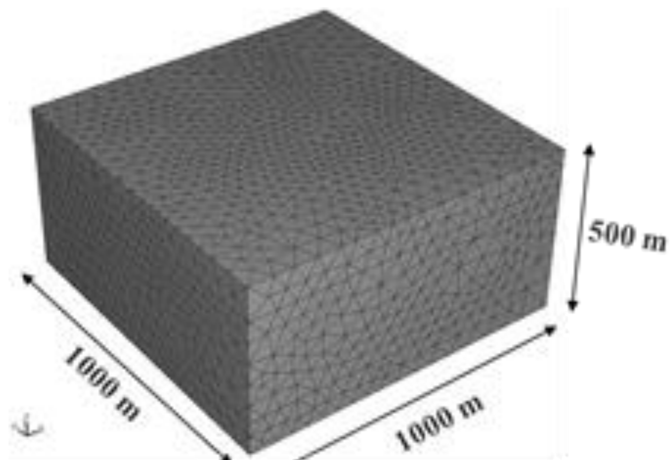

Fig. 4. Typical model – initial mesh.

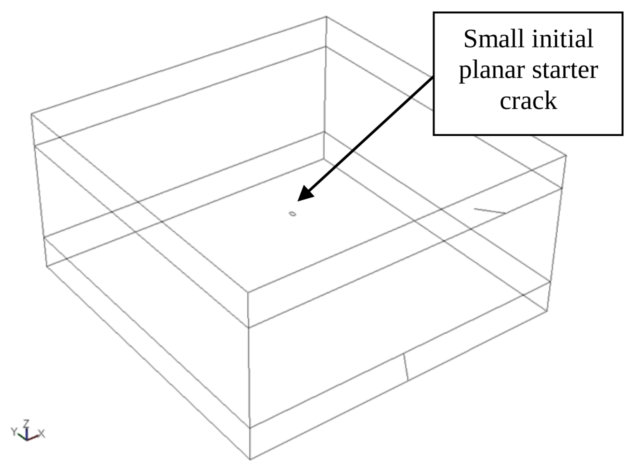

Fig. 5. Typical model – profile view.

The *prediction* stage determines the hydraulic fracture length and direction based on an accumulation of damage as computed by the CDM material model. The damage variable, which is a measure of the amount of strain-softening an element has undergone, is computed at the element centers as is standard practice in explicit finite element solvers; these points values (see Fig. 6) are subsequently accrued to form an annulus using a marching tetrahedral algorithm (see Fig. 7). Once the annulus is established it is smoothed using a convex hull approach which establishes an outer boundary skin. From the convex hull the extent of the damage area is determined by projecting outwards from the edge of the existing fracture (see Fig. 8).

The existing methodology requires that there be a parent-child relationship between the network nodes (implicit solver) and the fracture surface (explicit solver) nodes. This is necessary to ensure key variables, e.g. the fluid pressure and fluid leak-off, are transferred from nodes on the network element to corresponding nodes on the fracture surfaces. In effect a topological constraint is enforced on any new mesh in which mesh nodes on either side of a fracture must match. This is achieved by first converting the discrete matrix and fracture network into a continuum model in a process known as *stitching*.

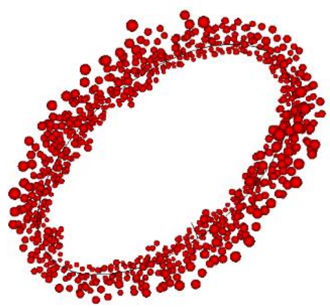

Fig. 6. Formation of 'point cloud' from material damage at element centres.

Fig. 7. Formation of annulus from point cloud damage.

From the continuum model all the fractures are represented as surfaces. Using the predicted extents it is possible to establish a new surface bound, then using the existing outer surface bound and the new extent bound a new surface is generated (see Fig. 9). This is the *insertion* stage.

The next stage is generating a new mesh based on the updated geometry (*meshing* stage). Remeshing is only performed locally (i.e. around the fracture tip) in an effort to reduce computational expense and avoid well-known global remeshing pitfalls such as dispersion of key material variables (e.g. the material damage).

After the *meshing* stage the model is still in a continuum form. This has to be returned to a discrete model to ensure the fractures are fully represented (*expansion* stage). As the remeshing is only performed locally at the fracture tip, the majority of the mapped variables (for variables defined both at mesh nodes and elements) will just be reset to values at their original configuration. It is only in the local newly remeshed regions where mapping is required between old and new meshes (*mapping* stage) (Peric et al, 1996**)**.

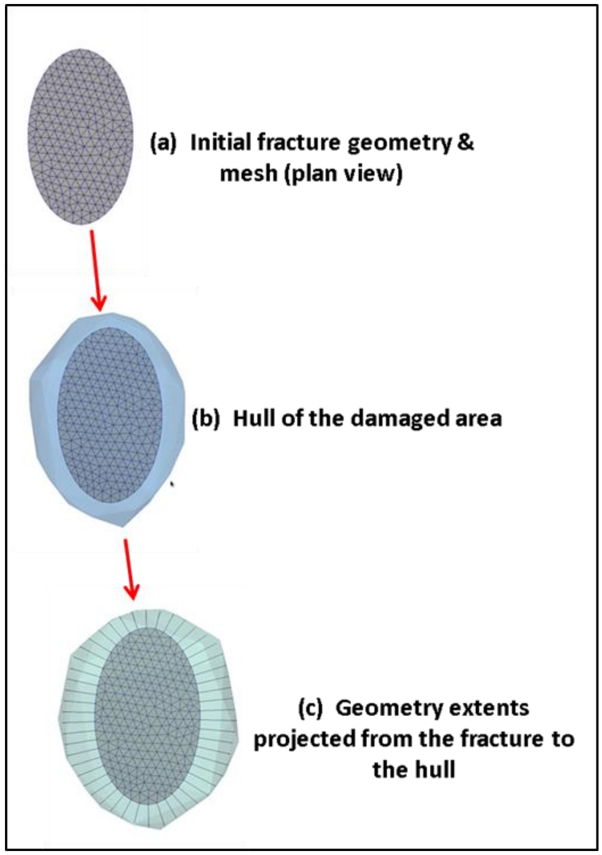

Fig. 8. Geometry extents projection from existing fracture

3. APPLICATIONS OF 3D ELFEN TGR

3.1. Overview of Applications

Two demonstration examples are presented:

- Curved fracture paths;
- Potentially connecting fractures;

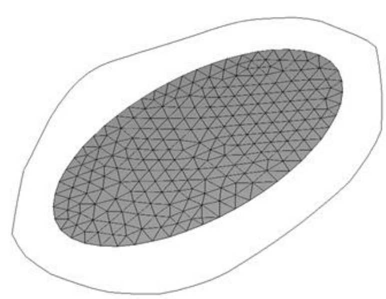

a. Bound of new surface given extents

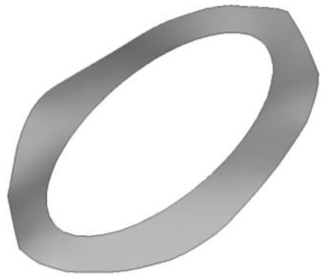

b. New geometry surface

Fig. 9. Insertion stage.

3.2. Material Properties

The isotropic elastic properties are shown in Table 1.

Table 1. Elastic properties

Material Parameter	Value
Young's modulus	32.0E9 Pa
Poisson's ratio	0.2

The continuum damage mechanics (CDM) material parameters to capture model-1 failure are described in Table 2.

Table 2. Fracture mechanics properties

Material Parameter	Value
Tensile strength	1.0E6 Pa
Fracture energy	50 Nm

3.3. Hydraulic Fracture Fluid Properties

The fracking fluid is assumed to be a Newtonian fluid with water-like viscosity (see Table 3).

Table 3. Fracking fluid properties

Fluid Parameter	Value
Viscosity	1.67E-3 Pa.s
Bulk fluid modulus	2.0E9 Pa

4. CASE STUDIES

4.1. Curving Hydraulic Fracturing

2D hydraulic fracture simulators are often prohibitive in their range of application due to a limiting plane strain or stress assumption. A full 3D simulator allows an analyst to assess the complex stress evolution in all 3 Cartesian directions. The point of application here is the curvature of a hydraulic fracture in response to a rotated (i.e. relative to the global axis) initial stress state.

Assuming that the horizontal wellbore is drilled non-parallel to the minimum principal stress (i.e. the least compressive stress), then the immediate fracture propagation is likely to curve relative to the wellbore rather than propagate in an orthogonal direction. This can have a key influence on the hydraulic fracture propagation, plus other key design components such as proppant transport and potential choking of the hydraulic fracture.

The initial geometry is shown in Fig. 10 with plan view dimensions of 250m x 250m (XY-plane) and a layer thickness of 100m. The fracking fluid is injected at a constant flow rate of $0.1\, m^3/s$ and it is assumed that the fracking fluid leak-off coefficient is very low. The minimum and maximum effective horizontal principal stresses are $-10E6\,Pa$ (σ_h') and $-17E6\,Pa$ (σ_H') respectively (negative implies compressive stress) with their corresponding principal directions shown in Fig. 10.

From Fig. 11 it can be observed that the horizontal fracture length is approximately 50m before it follows the most compressive horizontal stresses (i.e. the global field stresses). Fig. 12 shows a close-up of the fracture surface geometry evolution. Clearly, the fracture geometry is non-planar and is in contrast to the typical fracture geometry predicted by a 2D hydraulic fracture simulator suggesting the importance of a full 3D simulator to capture potentially complex fracturing.

4.2. Potentially Connecting Hydraulic Fractures

One of the most misunderstood areas of hydraulic fracturing is the stress shadow effect, where a complex evolving stress state between adjacent propagating hydraulic fractures could possibly shift the direction of one or both fractures, prevent one fracture from propagating or lead to fracture-fracture interference between multiple wells.

Since one of the goals of a successful hydraulic fracture job is the growth of balanced fractures from multiple wells and perforations to maximize stimulated rock volume while minimizing interference, understanding and quantifying this effect is essential. This is where the ELFEN TGR software becomes particularly useful.

The initial geometry is shown in Fig. 13 with plan view dimensions of 250m x 250m (XY-plane) and a layer thickness of 100m. The model contains two horizontal well stages spaced apart a horizontal distance (X-direction) of 35m and offset in the Y-direction by 30m. The fracking fluid is injected into both perforations contemporaneously at a constant flow rate of $0.05\, m^3/s$ with an assumed very low fracking fluid leak-off coefficient. The minimum and maximum effective horizontal principal stresses are $-10.7E6\,Pa$ (σ_h') and $-11E6\,Pa$ (σ_H') respectively with their corresponding principal directions shown in Fig. 13.

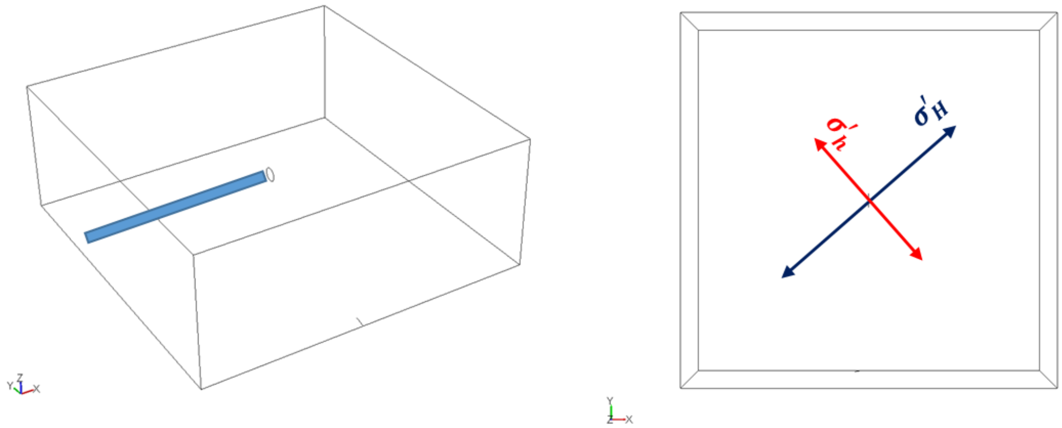

Projection view Plan view

Fig. 10. Initial model – curving hydraulic fracture case study

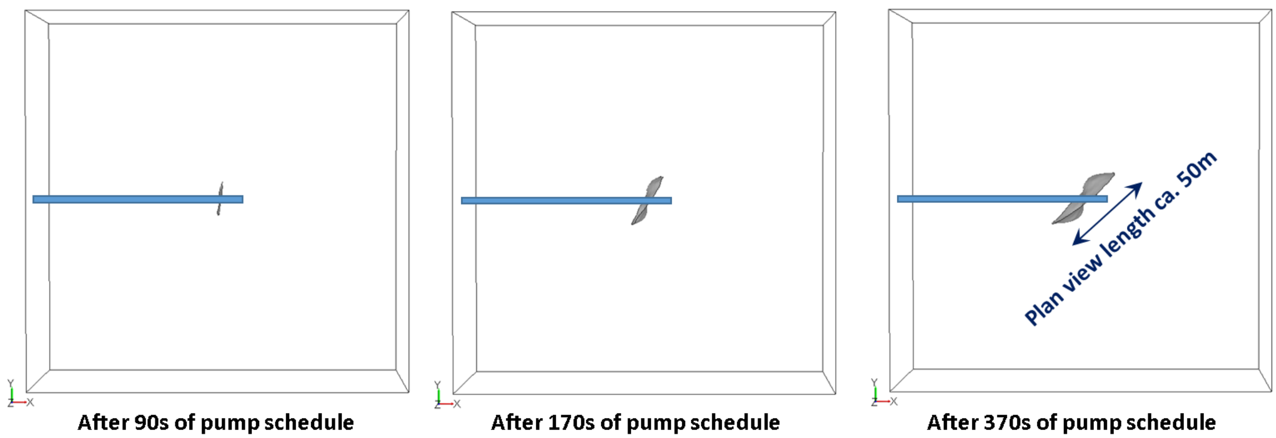

Fig. 11. Plan view propagation of curving fracture

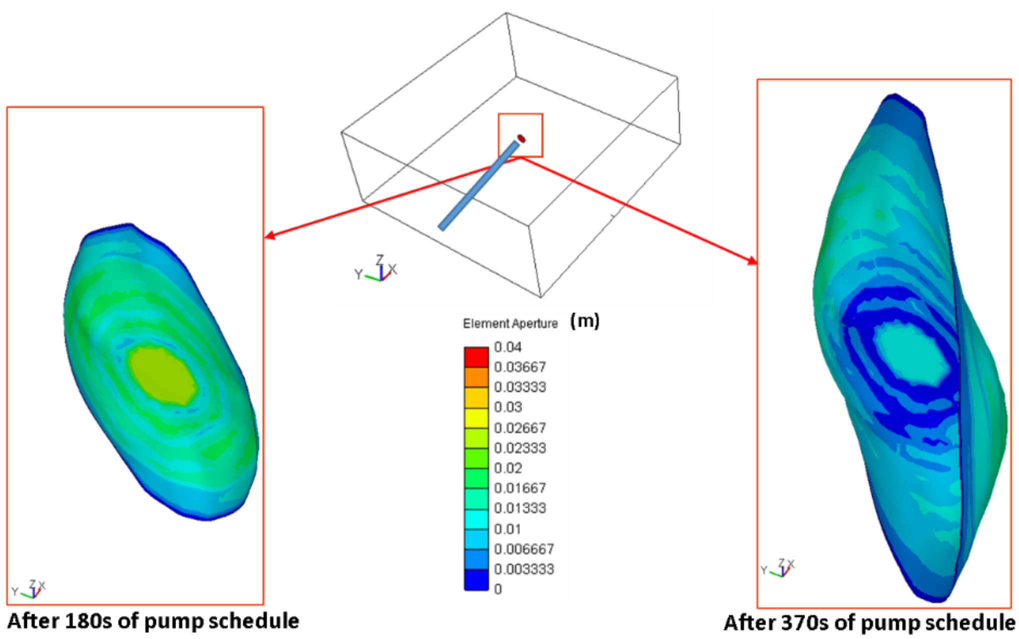

Fig. 12. Propagation of curving fracture with close-up of fracture geometry evolution along with element aperture

Fig. 14 shows the fracture evolution over the first 1200s of the pump schedule. Initially both fractures propagate towards the most compressive horizontal stress, but as the complex stress state evolves and each fracture perturbs the stress field, there is interaction between the pair. The stress interaction is a complex function of initial stress state, rock formation material properties, treatment schedule, fluid properties, proximity of wells/stages to each other and among others. Therefore it is very difficult to predict the possible fracture direction and understand cause and effects without advanced numerical simulation results. From Fig. 15 the extent of the stress bubble from pressurizing the hydraulic fracture is shown, via section cuts showing the least compressive principal stress. Finally, Fig. 16 shows the evolution of the tensile regions around the propagating hydraulic fracture, these are limited to a region adjacent to the propagating hydraulic fracture. The example presented here shows fracture propagation in an approximate isotropic in-situ stress state. If this was more anisotropic then the amount of fracture curvature could be increased as the propagating fracture tends to the most compressive horizontal stress σ'_H. This is further complicated by the interaction and resulting stress change as the stress bubbles (i.e. stress change from the in-situ stress) from the two propagating fractures overlap.

5. CONCLUSIONS

This paper has focused on the development of a new combined 3D Finite Element and Discrete Element method where fracture surfaces are inserted based on a geometry update procedure rather than the more traditional element splitting techniques. Modelling is built around a coupled geomechanical framework which monitors the formation stress evolution and the fluid pressure inside the propagating fracture. New fracture surface geometry is inserted when the Rankine yield criterion is satisfied for a threshold specified growth of material damage around the pressurised fracture, where the damage mainly accumulates at the fracture tips. In field case applications, increasing fracture complexity typically leads to enhanced production.

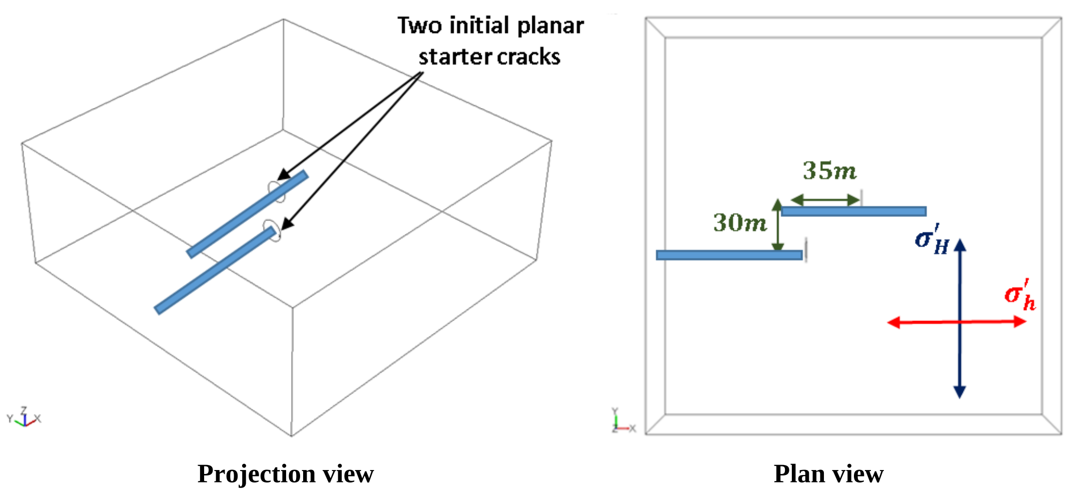

Fig. 13. Initial model - multi-cluster hydraulic fracturing case study

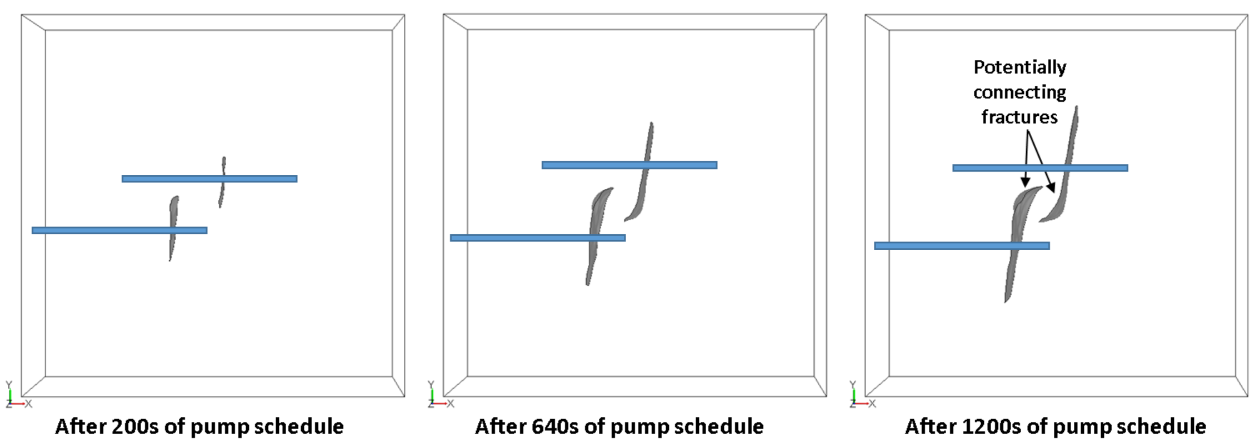

Fig. 14. Plan view propagation of potentially connecting fractures

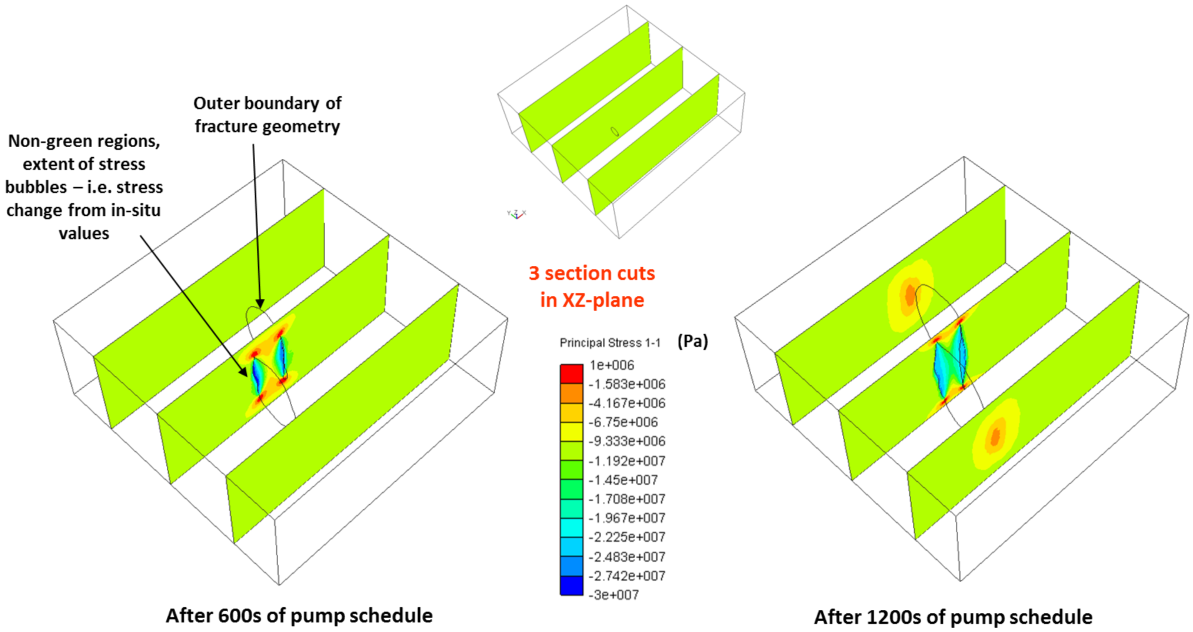

Fig. 15. Propagation of potentially connecting fractures along with least compressive principal stress

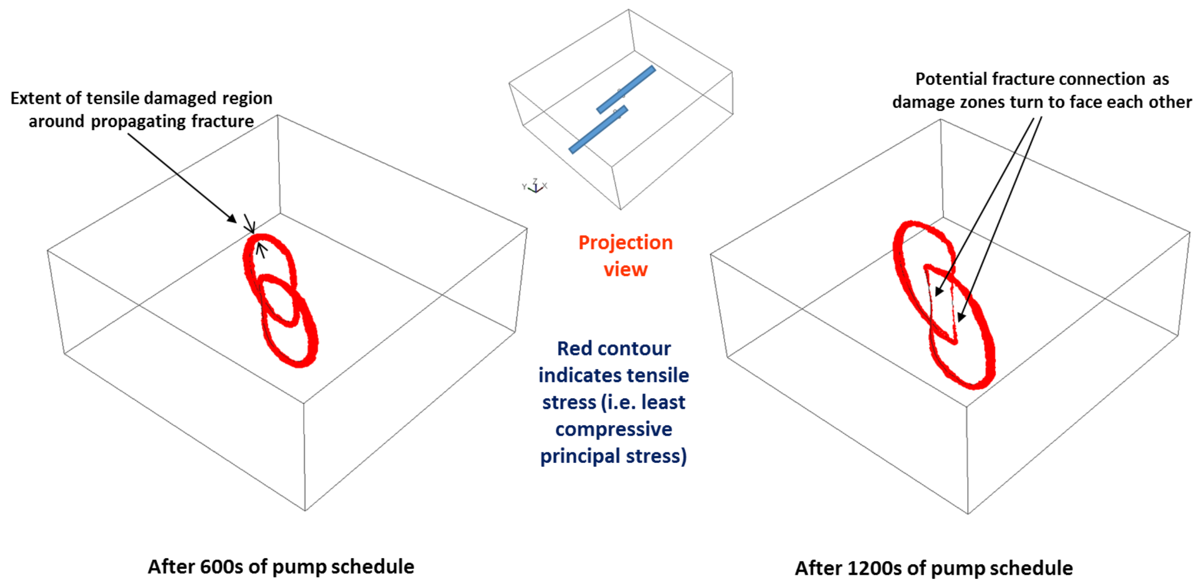

Fig. 16. Propagation of potentially connecting fractures along with extent of tensile stress (i.e. least compressive principal stress)

The fracture insertion process follows a 6-stage process to ensure that a good quality mesh is attained after the fracture is inserted, which is essential for the explicit solution of the mechanical stress field, whilst honouring the topology constraints between the network element nodes and the corresponding nodes on the fracture surfaces. A number of examples have been presented to illustrate the main functionality of the new 3D hydraulic fracture software tool. This has been highlighted via cases where curved fracture propagation from wellbores misaligned with respect to the least compressive stress and fracture interaction/curving between tightly spaced horizontal wells are simulated.

Future work includes using the ELFEN TGR to simulate the whole hydraulic stimulation process; including slurry, flowback and production stages.

REFERENCES

1. Bai, M. 2011. Improved understanding of fracturing tight-shale gas formations. In *Proceedings of the Production and Operation Symposium, Oklahoma City, Oklahoma 27 – 29 March 2011*, SPE 140968.

2. Bazant, P.Z. and J. Planas. 1997. *Fracture size effect in concrete and other quasi-brittle materials*. 1st ed. Wiley.

3. Belytschko, T., W.K. Liu and B. Moran. 2000. *Nonlinear finite elements for continua and structures*. 1st ed. Wiley.

4. Cipolla, C.L., N.R. Warpinski, M.J. Mayerhofer, E.P. Lolon, M.C. Vincent. 2010. The relationship between fracture complexity, reservoir properties and fracture-treatment design In *Proceedings of the Annual Technical Conference and Exhibition, Denver, Colorado 21 – 24 September 2010*, SPE 140253.

5. Crook, T., S.M. Willson, J.G. Yu, R. Owen. 2003. Computational modelling of the localized deformation associated with borehole breakout in quasi-brittle materials. *J. Petrol Sci. Eng.*. 38: 117–186.

6. Davies, R.J., S. Mathias, J. Moss, S. Hustoff. 2012. Hydraulic fractures: how far can they go? *Mar. Petrol Geol.*. 37: 1–6.

7. Economides, M.J. and K.G. Nolte. 2000. *Reservoir stimulation*. 3rd ed. Wiley.

8. Economides, M.J. and T. Martin. 2007. *Modern fracturing enhancing natural gas production*. Energy Tribune.

9. Gordeliey, E., A. Peirce. 2013. Coupling schemes for modelling hydraulic fracture propagation using the XFEM. *Comput. Method Appl.* M. 253: 305–322.

10. Huang, M., S. Wu, O.C. Zienkiewicz. 2001. Incompressible or nearly incompressible soil dynamic behaviour – a new staggered algorithm to circumvent restrictions of mixed formulations. *Soil Dyn. Earth Eng.* 21: 169–179.

11. Jones, J. and J.Z. Britt. 2006. *Design and appraisal of hydraulic fractures*. Society of Petroleum Engineers.

12. King, G.E. 2010. Thirty years of gas shale fracturing: what have we learned? In *Proceedings of the SPE Annual Technical Conference and Exhibition, Florence, Italy 19 – 22 September 2010*, SPE 133456.

13. Klerck, P.A. 2000. The finite element modeling of discrete fracture in quasi-brittle materials. Ph.D. Thesis, Swansea University

14. Labao, M.C. 2007. Finite element modeling of hydraulic fracture flow in porous media. Ph.D. Thesis, Swansea University

15. Lewis, R.W. and J.Z. Schrefler. 1998. *The finite element method in the static and dynamic deformation and consolidation of porous media*. 2nd ed. Wiley.

16. Munjiza, A. 2004. *Combined finite-discrete element method*. 1st ed. Wiley.

17. Peric, D., C.H. Hochard, M. Dutko., D.R.J. Owen. 1996. Transfer operators for evolving meshes in small strain elasto-plasticity. *Comput. Methods Appl. Mech. Engrg.* 137: 331–344.

18. Profit, M., M. Dutko, J. Yu., S. Cole, D. Angus, A. Baird. 2015. Complementary hydro-mechancial coupled finite/discrete element and microseismic modelling to predict hydraulic fracture propagation in tight shale reservoirs. *Comp. Part. Mech.* pre-print.

19. Rockfield Software Ltd. 2014. ELFEN TGR Manual.

20. Soliman, M.Y., J. Augustine. 2010. Fracturing design aimed at enhancing fracture complexity In *Proceedings of the Annual Conference, Barcelona, Spain 14 – 17 June 2010*, SPE 130043.

21. Williams, B.B. 1970. Fluid loss from hydraulically induced fractures. *J. Pet. Tech.* 22: 882–888.

22. Wu, S.R. and L. Giu. 2012. *Introduction to the explicit finite element method for nonlinear transient dynamics*. 1st ed. Wiley.

23. Yew, C.H. and X. Weng. 2015. *Design and appraisal of hydraulic fractures*. 2nd ed. Society of Petroleum Engineers.

24. Zienkiewicz, O.C., R.L. Taylor and J.Z. Zhu. 2005. 6th ed. Butterworth-Heinemann.